Published in IET Science, Measurement and Technology
Received on 17th December 2010
Revised on 15th May 2011
doi: 10.1049/iet-smt.2010.0170

ISSN 1751-8822

Cryogenic current comparators and their application to electrical metrology

*J.M. Williams**

National Physical Laboratory, Teddington TW11 0LW, UK
**School of Engineering and Mathematical Sciences, City University, London EC1V 0HB, UK*
E-mail: jonathan.williams@npl.co.uk

Abstract: The cryogenic current comparator (CCC), first demonstrated nearly 40 years ago, has become a key component of electrical metrology. It utilises a superconducting screen to achieve very high ratio accuracy and hence has found many applications where the electrical units need to be scaled over decade values. It has been deployed over a wide range of currents from 100 A to 1 pA and has been used to verify the accuracy of electrical quantum effects such as the quantised Hall effect. This study is a review of the theory, design principles and most common applications of the CCC. In addition to the summary of its use in top-level electrical metrology, some recent developments such as the use of high temperature superconducting materials and applications outside the realisation of electrical units are described.

1 Introduction

The cryogenic current comparator (CCC) is a device for comparing two electrical currents. In a CCC, a superconducting screen surrounds the current-carrying conductors and separates them from a magnetic flux null detector, normally a superconducting quantum interference device (SQUID) [1]. When carefully constructed, the superconducting screen attenuates magnetic field components arising from the position of the conductors within the screen to a very high level. In this situation, the resultant flux is proportional to the difference between the products of current and turns number, enabling the current ratio to be determined and adjusted with a relative accuracy of better than 1 part in 10^{10} in a well-constructed device. By appropriate choice of winding ratios, current ratios from 1:1 to more than 10 000:1 can be established. The CCC thus provides a very accurate way of scaling the electrical units of current, voltage and resistance and has become an essential component of precision electrical metrology.

The status of electrical metrology and its associated measurement techniques has been covered in a number of review articles [2, 3] and the use of SQUIDs and the CCC as measurement tools has been summarised in a book chapter [4]. The aim of this review is to describe the role of the CCC in the development of electrical metrology in more detail and to summarise the different design approaches and their application to different problems. The review is organised as follows: Section 2 outlines the basic principle of the CCC and its first realisation, Section 3 describes the design approaches for CCCs and the method of testing their accuracy, Section 4 presents the application of the CCC to a wide range of electrical metrology, Section 5 reviews the introduction of high temperature superconductor (HTS) materials into CCCs and some applications outside mainstream electrical metrology.

2 Basic principle of a CCC

The basic principle of a CCC can be understood by considering a simple tube of superconducting material surrounding two current-carrying wires as illustrated in Fig. 1. Magnetic flux is excluded from the superconductor by the Meissner effect, so a current in any one of the conductors induces an identical counter current on the inside surface of the screen which then returns via the outside surface. The current distribution varies around the circumference of the tube but Ampere's law dictates that the sum of all the screening current filaments plus I_1 and I_2 must be zero, thus $I_1 - I_2 = I_S$. On the inside surface, the current distribution is influenced by the position of the conductors but on the outside surface, away from the ends of the tube, the current distribution becomes progressively more uniform and the influence of the position of the conductors diminishes. This is the essential feature of the CCC and the position independence allows currents to be compared with high accuracy. Specifically, if the magnetic field generated by I_S is sensed with a magnetic flux detector or superconducting pick-up coil positioned away from the tube ends as illustrated in Fig. 1, then zero detected flux indicates that $I_1 = I_2$. A 1:N current ratio can be achieved by having N conductors in the tube carrying current I_2 with a single conductor carrying I_1 so that $I_1 - NI_2 = I_S$.

In the original design, the non-ideal behaviour at the ends of the shield was accommodated by taking the tube ends to a far distance and employing a second overall screening tube to reduce stray fields in the detection region to a negligible level [5]. The sensitivity of the comparator was enhanced by

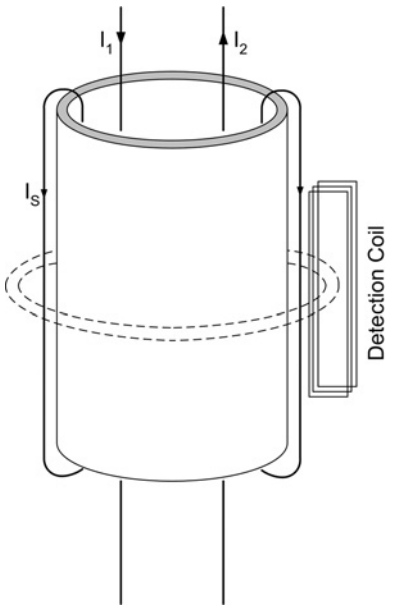

Fig. 1 *General principle of a CCC*

bending the tubular shield, with the wires inside, into the shape of a coil. The accuracy achieved for the comparison of equal currents with this approach was in the range 1.0 to 2.5×10^{-8}. The main limitations of this design approach are that integer current ratios higher than about 10:1 become difficult to achieve since progressively more conductors are required inside the tube, and schemes with larger numbers of turns of the tube around the detection coil to achieve a higher sensitivity for small currents are difficult to construct. For this reason, two different approaches to the resolution of the non-ideal behaviour at the ends of the superconducting tube were adopted, as illustrated in Fig. 2.

The first approach [6] forms a single turn loop of the tubular shield and overlaps one tube end into the other. The ends of the conductors forming the ratio winding are taken out through a side tube attached to the main shield. To achieve the necessary attenuation of the field at the tube ends, the tube is overlapped more than once and so a series of coaxial exit tubes is constructed, one for each overlap. The second approach [7] effectively stretches open the ends of the tubular shield and bends them back over the detection area. The ends of the tube are again accommodated by an overlap system resulting in toroidal shield geometry. This time an exit tube is needed for the detector coil, since this is now on the inside of the shield and the ratio winding on the outside. Once again, a coaxial exit tube is constructed for each shield overlap. The first design with the ratio windings inside the screen and the detection area outside has become known as a Type I CCC and the opposite topology with the ratio windings outside the screen as a Type II CCC. It can be seen that both topologies permit assembly of ratio windings with high ratios and large numbers of turns.

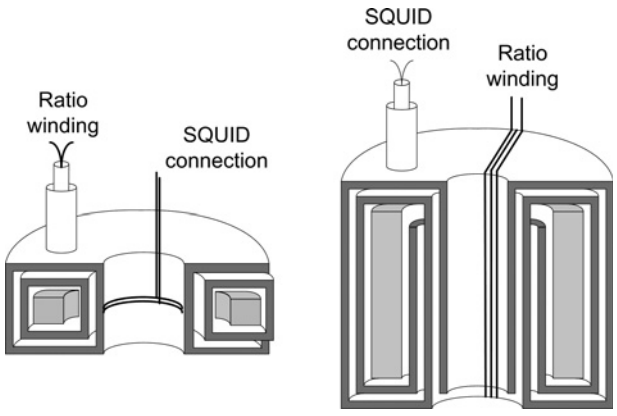

Fig. 2 *Schematic diagrams of the Type I (left) and Type II (right) CCC geometries*

In the Type I design, the ratio windings form a circular coil, represented by the grey central region of square cross-section, and the wires are perpendicular to the page at the plane of the cut. The pick-up coil is also circular and is mounted outside the shield in the centre of the torus. In the Type II design, the pick-up winding is a torroidal coil wound around a former, represented by the grey half-ring at the centre and the ratio windings are wound on the outside of the shield, also with toroidal geometry

3 Design, construction and testing

3.1 Calculation of CCC sensitivity

A key parameter of a CCC is its sensitivity for current measurement, which can be expressed as an equivalent input current noise. A SQUID and an appropriately constructed superconducting pick-up coil is the most commonly used detection arrangement in a CCC assembly. The noise performance of a SQUID is commonly expressed in terms of its energy resolution $\langle \varepsilon \rangle$ and this can be related to an equivalent current noise i_S

$$\langle i_S^2 \rangle = \frac{2\langle \varepsilon \rangle}{L_S} \tag{1}$$

where L_S is the inductance of the SQUID coil (normally set by the manufacturer) and the brackets denote a time-averaged or expectation value. The sensitivity of the CCC is governed by this energy resolution and the matching of the SQUID inductance to the inductance of the CCC tubular shield.

Both Type I and Type II CCCs can be evaluated using the same approach and the equivalent electrical circuit for the CCC with a pick-up coil connected to a SQUID coil is shown in Fig. 3, where L_P and L_T are the inductances of the pick-up coil and CCC tubular shield, respectively. The ratio, α, of the current in the SQUID input coil, i_S, to the total current flowing on the CCC shield, i_T, and its optimum value, α_m, which occurs at $L_P = L_S$, are easily shown to be [8]

$$\alpha = \frac{i_S}{i_T} = \frac{k(L_T L_P)^{(1/2)}}{L_S + L_P}, \quad \alpha_m = \frac{k}{2}\left(\frac{L_T}{L_S}\right)^{(1/2)} \tag{2}$$

where k is the coupling constant between the shield and the pick-up coil.

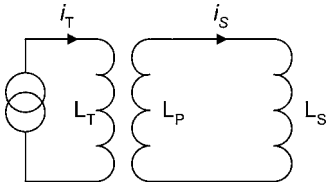

Fig. 3 *Equivalent circuit showing a constant current, i_T, flowing on the CCC shield, L_T, with a mutual inductance to the pick-up coil, L_P*

doi: 10.1049/iet-smt.2010.0170

Assuming that the pick-up coil is matched to the SQUID input coil, then α_m can be used to deduce an equivalent current noise, $i_{n,}$ for a single turn on the CCC, which depends only on the inductance of the torus

$$\langle i_n^2 \rangle = \frac{8\langle \varepsilon \rangle}{k^2 L_T} \tag{3}$$

An energy resolution of 10^{-31} Js for a typical commercially available SQUID and a typical torus inductance of 50 nH gives a value of $i_n = 4\,\text{pA}/\sqrt{\text{Hz}}$ for a single turn.

The performance of a SQUID is also expressed in terms of flux noise Φ_n as a fraction of the magnetic flux quantum Φ_0. To relate this to an equivalent current noise, the coupling coefficient between the SQUID input coil and the SQUID loop itself, normally quoted in terms of a parameter M with units of $\Phi_0 A^{-1}$, is also required. Equation (3) then becomes

$$\langle i_n^2 \rangle = \frac{4\langle \Phi_n^2 \rangle}{k^2 L_T} \times \frac{L_S}{M^2} \tag{4}$$

The two parameters L_S and M^2 are normally related in a SQUID design so that their ratio needs to be considered as a figure-of-merit. Typical values of $L_S = 1.1\ \mu\text{H}$, $1/M = 0.13\ \mu\text{A}\Phi_0^{-1}$, and $\Phi_n = 3\ \mu\Phi_0/\sqrt{\text{Hz}}$, again gives a value of $i_n = 4\ \text{pA}/\sqrt{\text{Hz}}$. It should be noted that this value for i_n is about a factor of 10 worse than the equivalent input current noise of the SQUID at the input coil, i_S. This is due to the mismatch between the torus inductance and the SQUID input coil inductance, also a factor of 2 that comes from the series circuit of the pick-up coil and the SQUID input coil, often referred to as a 'flux transformer'.

The basic noise of a SQUID is normally quoted by the manufacturer for a bandwidth of 1 Hz at a frequency in the kHz range. All SQUIDs, however, suffer from $1/f$ noise which becomes significant at measurement frequencies below 10 Hz. Fig. 4 is a plot of the measured noise on an example commercial dc SQUID. The noise is plotted as an Allan deviation [9] and the onset of $1/f$ noise is indicated by the change of the graph slope from $1/\sqrt{\tau}$ to horizontal. For the SQUID in this example, this occurs at approximately 6 s. The presence of $1/f$ noise means that averaging for longer measurement intervals does not lead to a lower standard deviation. The only way to achieve a higher measurement resolution is to modulate the signal; in the case of a CCC this is achieved by simultaneously reversing the two measurement currents.

3.2 Type I: design considerations

In a Type I design the pick-up coil normally consists of a few turns wound as a short solenoid. The inductance of this geometry can be estimated from the formula [10]

$$L_P = N^2 \mu_0 b[\ln(8b/\rho) - 2] \tag{5}$$

where N is the number of turns, b is the radius of the coil, ρ is the radius of the wire and μ_0 is the permeability in free space. The inductance of the CCC shield can similarly be calculated from (5) with $N = 1$ within the assumption that the shape of the cross-section does not have a dramatic effect on the inductance [11]. For the CCC in [10] with $b = 15.9$ mm, $\rho = 0.065$ mm, $N = 4$ and CCC radius and cross-section radius of 18.5 mm and 2.5 mm, respectively, $L_P = 1.8\ \mu\text{H}$ to match the SQUID coil inductance L_S of approximately 2 μH and $L_T = 48$ nH. This gives a value of $\alpha_m = 0.077$ and a sensitivity for a single turn of 2.6 μA Φ_0^{-1} assuming a SQUID input sensitivity in this case of 0.2 μA Φ_0^{-1} and that $k = 1$. The strong coupling between the pick-up coil and the CCC shield modifies its effective inductance to be [12]

$$L_p' = L_p(1 - k') + kN^2 L_T \tag{6}$$

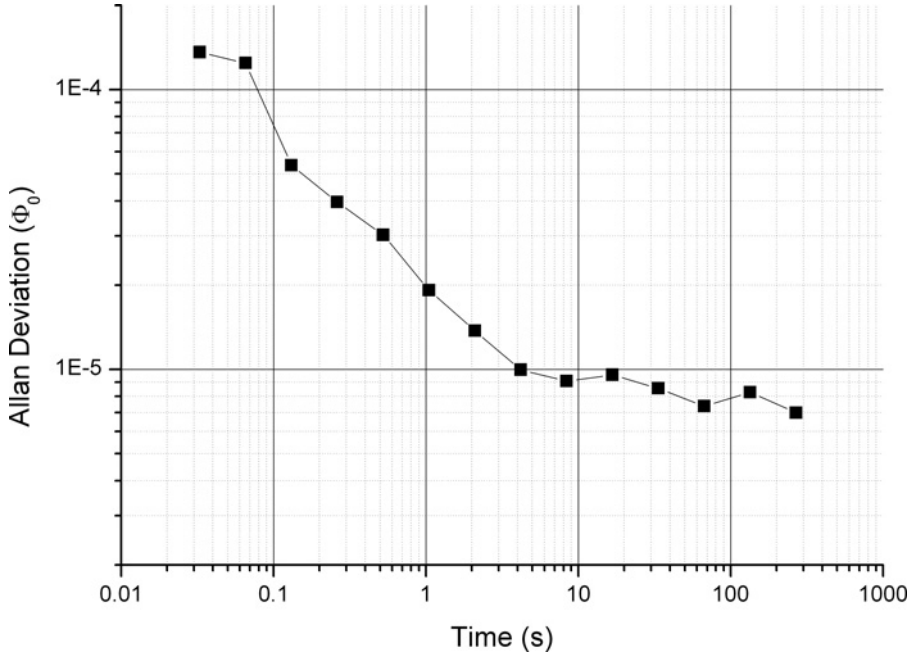

Fig. 4 *Allan deviation for a typical SQUID*
Allan deviation at 1 s corresponds to a white noise of 30 $\mu\phi_0/\sqrt{\text{Hz}}$

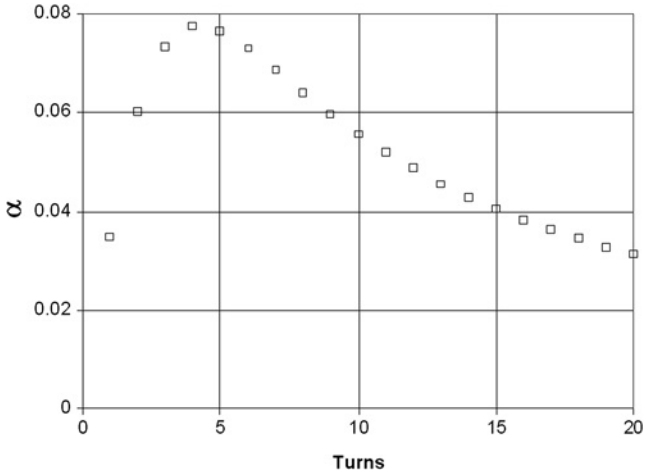

Fig. 5 *Variation in CCC coupling factor α with number of turns on the pick-up winding*

where k' is the coupling between the pick-up coil and its image in the CCC shield. In the limit where $k' = 1$, the effective inductance of the pick-up coil is determined by its number of turns and the inductance of the CCC shield. Under these conditions, the optimum value of α is still α_m given in (2), but now the optimum number of turns is given simply by

$$N_m = \sqrt{L_S/L_T} \quad \text{and} \quad \alpha_m = k/(2N_m) \tag{7}$$

For the numerical example above, this revised treatment gives $N_m = 6.5$ and $\alpha_m = 0.077$, whereas four turns would give $\alpha = 0.069$, a difference of just 10%. In fact alpha varies slowly with N around the maximum, as illustrated in Fig. 5, and the sensitivity is within 94% of α_m for values of N between 3 and 6. The largest value of α_m possible is 0.5 and occurs for the limiting case where the pick-up coil has just one turn and the CCC shield is sufficiently large that $L_T = L_S$.

A further factor for the Type-I CCC is the influence of the overall external shield that can reduce the effective inductance of the CCC shield, L_T. An external shield is required because the pick-up coil is on the outside of the CCC and is therefore susceptible to stray fields. A model which considers the dependence of CCC shield inductance, L_T, on the dimensions of the overall shield shows that, for a given overall shield radius, α, first increases with the radius of the CCC shield as L_T increases but reaches a maximum before decreasing as the shield starts to reduce the effective value of L_T [13]. A formulation of this problem using a method of magnetic reluctance leads to an intuitive understanding of how the shield modifies L_T and a simple 'rule of thumb' that the optimum inductance for a given external shield radius is obtained when the area described by the hole at the centre of the torus equals the area described by the ring between the outside of the torus and inside of the shield [14]. A very detailed numerical model, which takes account of all aspects including the pick-up coil and overall shield, gives values for α which are within a few per cent of measured values for a range of CCC designs [15], confirming that the performance of Type I designs is now well understood.

A SQUID with low input inductance can be connected directly to the CCC torus [16]. A separate pick-up coil is not required and the coupling is perfect, corresponding to (4) with $k = 1$. However, the efficiency still relies on the matching of the SQUID input coil to the torus inductance and on the interconnecting wires having very low inductance, α reaching the maximum value of $\alpha_m = 0.5$ when the inductances are matched and the inductance of the connecting wires is negligible. The specifications given in [16] for this approach are $L_T = 59$ nH, $L_S = 45$ nH, $1/M = 1.1$ μA/Φ_0 and a measured sensitivity of 2.3 μA/Φ_0 for a single turn, corresponding to value of $\alpha = 0.48$, which is very close to the theoretical maximum. This CCC will be discussed further in the section on high value resistors and small currents.

3.3 Type II: design considerations

The design considerations for a Type II CCC are simpler in concept. An overall external shield is not required since the pick-up winding is on the inside of the CCC shield and is screened from external magnetic fields. The equations for matching the pick-up coil to the SQUID input coil inductance are the same as for the Type I design and the inductances of the shield and coil are calculated using the formula for a toroidal geometry

$$L = \frac{\mu_0 h n^2}{2\pi} \ln\left(\frac{b}{a}\right) \tag{8}$$

where h is the height, a is the inner radius and b is the outer radius. A compact Type II CCC designed to be used in a transport helium cryostat with a 50 mm neck diameter [8] had shield dimensions of $a = 14$ mm, $b = 16$ mm and $h = 45$ mm. This gives an inductance of $L = 1.2$ nH and a corresponding value $\alpha_m = 0.012$ for a SQUID input coil inductance of 2 μH. To put this into context, a Type-I CCC occupying a similar volume would have an overall outer screen radius of 20 mm and applying the equal area principle described above would have a CCC radius of 13 mm for a cross-section radius of 5 mm (a radius of 5 mm is typical for most Type I designs in comparison with the figure of 2.5 mm achieved in [10]). Equation (5) with these values gives $L_T = 17$ nH and a corresponding value $\alpha_m = 0.05$ which is approximately four times better than the Type II design.

Thus for a given volume, the Type I design will be more sensitive and its sensitivity increases linearly with radius whereas the Type II sensitivity is virtually independent of radius, being proportional instead to the height. The majority of CCC devices constructed have been of the Type I design but the Type II version has some advantages in special applications, including comparators for high currents and also for alternating current as will be described later.

3.4 Estimation of CCC error

In both the Type I and Type II designs, the open ends of the superconducting screen are closed by one end becoming coaxial within the other. The entry into the coaxial region and cross-section showing the cylindrical coordinate system (r, ϕ, z) are shown in Fig. 6. In a practical design, the width of the overlap region is small in comparison with the tube radius but has been enlarged in the figure for clarity.

To estimate the error of CCC, it is necessary to establish (i) the coupling, θ_1, between the magnetic field, B, generated by

doi: 10.1049/iet-smt.2010.0170

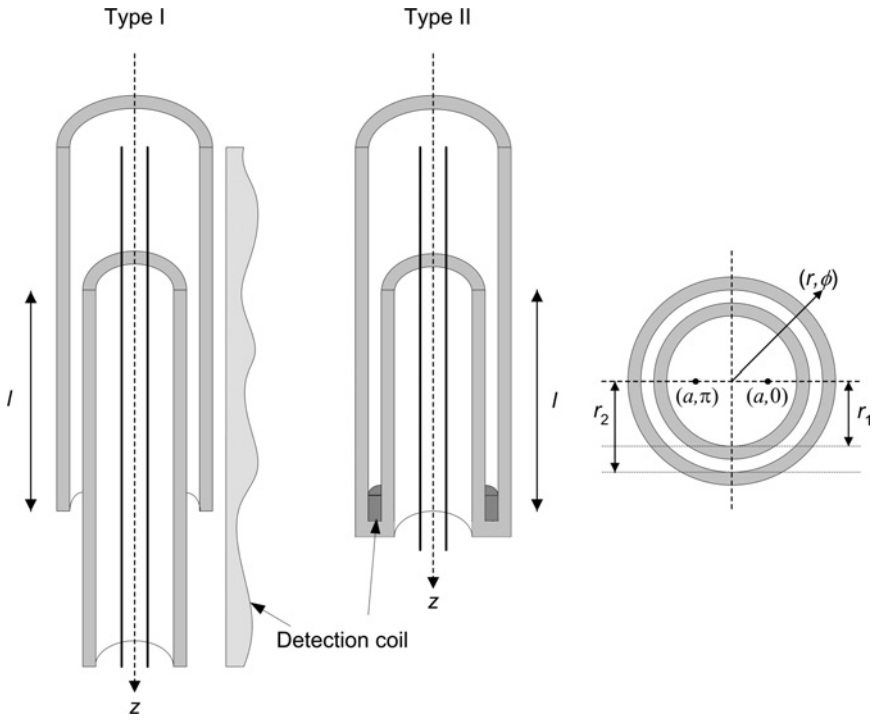

Fig. 6 *Cut away view of a CCC shield showing entrance to the coaxial region*

Location of the detection coil is in the plane of the paper for the Type I geometry and is toroidal for the Type II geometry. The cross-section shows the position of the current-carrying wires and cylindrical coordinate system. The thickness of the screens and width of the gap have been exaggerated for clarity

the two current-carrying wires in the superconducting tube and the field in the coaxial region, (ii) the attenuation, θ_2, of the field as it propagates from one end of the coaxial region to the other and (iii) the geometry factor, A, describing the eventual magnetic flux threading the pick-up coil at the end of the coaxial region which has dimensions of area. The same approach can be used for estimating the factors θ_1 and θ_2 for both types of CCC design.

The CCC error is the product of these three factors and will be zero if any of the factors is zero. In practice however, none of them can be made exactly zero since the two current-carrying wires can never occupy exactly the same space, the coaxial region cannot be infinitely long and the pick-up coil cannot be made with perfect symmetry. The following is a summary of how these three components can be modelled and estimated in a practical design.

In general, a magnetic field B can described by a scalar potential such that $B = \nabla V$ and V satisfies the Laplace equation in cylindrical polar coordinates

$$\frac{1}{r}\frac{\partial}{\partial r}\left(r\frac{\partial V}{\partial r}\right)+\frac{1}{r^2}\frac{\partial^2 V}{\partial \phi^2}+\frac{\partial^2 V}{\partial z^2}=0$$

For a centrally positioned wire on the axis of the tube, carrying a current I, the potential far away from the ends is

$$V=\frac{\mu_0 I}{2\pi}\phi$$

and the corresponding field has only one component

$$B_\phi(r)=\frac{1}{r}\frac{\partial V}{\partial \phi}=\frac{\mu_0 I}{2\pi r}$$

For the case where the two current-carrying wires carry equal and opposite current, I, are symmetrically placed on the $\phi = 0$ axis at a distance a from the centre of a tube of inner radius r_0, the potential far away from the tube ends can be expressed in terms of cylindrical harmonics [17]

$$V(r,\phi)=-\frac{\mu_0 I}{2\pi}\left\{\sum_{n=1}^{\infty}\frac{2}{2n-1}\left[\left(\frac{a}{r}\right)^{2n-1}+\left(\frac{a}{r_0}\times\frac{r}{r_0}\right)^{2n-1}\right]\sin(2n-1)\phi\right\}$$

The field again only has one component

$$B_\phi(r)=-\frac{\mu_0 I}{\pi r}\left\{\sum_{n=1}^{\infty}\left[\left(\frac{a}{r}\right)^{2n-1}+\left(\frac{a}{r_0}\times\frac{r}{r_0}\right)^{2n-1}\right]\cos(2n-1)\phi\right\}$$

This satisfies the boundary condition that the magnetic field normal to the surface of the superconducting tube is everywhere zero since $\partial V/\partial r = 0$ at $r = r_0$. As the currents are equal and opposite, the term $\mu_0 I\phi/2\pi$ for the two wires has cancelled and the symmetry of the position of the wires means that there are no even components so the series has the index $2n - 1$ and for an infinite tube, the potential and field are independent of z.

The solution in the coaxial region is more complex than in the plain tube and is also z-dependent. The boundary conditions for the region between the two cylinders dictate that the normal component of the field to the superconducting surface is zero at both $r = r_1$, the outside surface of the inner cylinder, and $r = r_2$, the inside surface of the outer cylinder. This is only satisfied by a potential

given by the Bessel function solution

$$V(r,\phi,z)=\sum_{n=1}^{\infty}\sum_{p=1}^{\infty}A_{np}[J_n(k_p^n r)+B_nY_n(k_p^n r)][C_{np}e^{+k_p^n z}+e^{-k_p^n z}]\sin(n\phi)$$

With associated eigenvalue equation (prime denotes derivative)

$$J_n'(k_p^n r_1)Y_n'(k_p^n r_2)-J_n'(k_p^n r_2)Y_n'(k_p^n r_1)=0$$

where k_{p}^n has p values for each n.

The boundary condition also determines B_n so the expression for the potential becomes

$$V(r,\phi,z)=\sum_{n=1}^{\infty}\sum_{p=1}^{\infty}D_{np}[J_n(k_p^n r)Y_n'(k_p^n r_1)-J_n'(k_p^n r_1)Y_n(k_p^n r)][C_{np}e^{+k_p^n z}+e^{-k_p^n z}]\sin(n\phi)$$

where $D_{np}=A_{np}/Y_n'(k_p^n r_1)$. The constants D_{np} and C_{np} are determined by considering the boundary conditions at the entrance and exit of the coaxial region, respectively. Writing $x=k_p^n r_1$ and $\beta x=k_p^n r_2$, the eigenvalue equation takes the standard form

$$J_n'(x)Y_n'(\beta x)-J_n'(\beta x)Y_n'(x)=0$$

for which numerical solutions exist for specific values of β [18]. Values for βx_p^n for $\beta=1.1$ are given in Table 1 for the first few values of n and p.

The different modes decay exponentially as they propagate along the coaxial region with exponents of $\beta x_p^n z/r_2$ [19]. It can be seen that for the case $\beta=1.1$ the modes with $p>1$ decay very rapidly so can be neglected. For $p=1$, the modes decay with an attenuation factor approximately proportional to n, so for distances greater than $l\sim 2r_2$ the higher order terms will be less than 10%. Thus, for estimating the error of a CCC, only the $n=1$, $p=1$ term needs to be considered. The dominance of this term has been demonstrated in a Type II design using a set of 12 test wires equally spaced around the tube circumference. The CCC error was found to vary sinusoidally with the pair of wires energised as expected [17]. The relevant attenuation coefficient for θ_2 is therefore the one corresponding to k_1^1 and for the example of $\beta=1.1$ above will be

$$\theta_2=e^{-1.05l/r_2}$$

For estimating θ_1, the $n=1$ case again only need to be considered. Thus, the magnetic field, at the coaxial gap entrance, close to the wall for two symmetrically placed wires carrying equal and opposite currents is

$$B_{1\phi}(r=r_0)=-\frac{\mu_0 I}{\pi r_0}\left(\frac{2a}{r_0}\right)\cos\phi$$

to be compared with the field for a single centrally placed wire

$$B_{2\phi}(r=r_0)=-\frac{\mu_0 I}{2\pi r_0}$$

In calculating the coupling from the tube into the coaxial region, there is the complication that there are two radii involved, r_1 and r_2 rather than just r_0. However, a detailed analysis reveals that for β close to unity, the coupling coefficient is close to unity ((6) of [20]). Thus

$$\theta_1=\frac{4a}{r_0}\cos\phi$$

For a Type I CCC, where the tube is conceptually bent round into a toroidal shape, a centrally placed wire in the superconducting tube carrying current, I, causes a uniform surface current of total value, I, to flow on the surface of the torus. The total flux threading the torus and hence the pick-up coil is [20]

$$\Phi_1=\mu_0 I R_{\mathrm{T}}\ \ln\left(R_{\mathrm{T}}/R_a\right)$$

where R_{T} is the radius of the torus and R_a is the radius of the cross-section. The field from a centrally placed wire propagates through the coaxial region without attenuation so writing

$$\Phi_1=\frac{\mu_0 I}{2\pi r_0}\times A_1$$

we have $A_1=2\pi r_0 R_{\mathrm{T}}\ln(R_{\mathrm{T}}/R_a)$.

For the two symmetrically placed wires

$$\Phi_2=\frac{\mu_0 I}{2\pi r_0}(\theta_1\theta_2 A_2)$$

and as calculated in [20] $A_2=2r_0(r_2-r_1)$.

Thus, finally the maximum ratio error of a Type I CCC (corresponding to $\phi=0$) is expressed as ratio of the flux in the pick-up coil for two wires carrying equal and opposite current, so a single centrally placed wire carrying the same current is

$$\frac{\Phi_2}{\Phi_1}=\frac{\theta_1\theta_2 A_2}{A_1}=\frac{4a}{r_0}(e^{-1.05l/r_0})\frac{(r_2-r_1)}{\pi R_{\mathrm{T}}\ln\left(R_{\mathrm{T}}/R_a\right)}$$

The term A_2/A_1 gives a useful factor of 1/1000 in a practical design but the remainder of the accuracy has to come from the exponential decay in the coaxial region. For an overall accuracy of 1 part in 10^{10}, the attenuation in the coaxial region needs to be at least 10^{-7} corresponding to $l/r_0>16$. In a typical Type I design, the radius of the torus is about twice the radius of the shield cross-section, so for a ratio of 16, the coaxial overlap region needs to be at least 1.5× the torus circumference.

For a Type II CCC, the coupling to the pick-up coil is different and depends on the uniformity of the coil [17]. Another consideration is that the attenuation in the coaxial

Table 1 Values of βx_p^n for $\beta=1.1$

p	1	2	3	4
n				
1	1.05	34.6	69.1	104
2	2.10	34.6	69.2	104
3	3.14	34.7	69.2	104
4	4.19	34.8	69.2	104

doi: 10.1049/iet-smt.2010.0170

region is much stronger for the sections parallel to the CCC axis than for the tangential sections [21]. It is thus advantageous to make a Type II CCC tall and narrow – for example, if its height is three times its radius then three shield overlaps will achieve $l/r_0 = 18$.

3.5 Measurement of CCC error

Although the accuracy of a CCC can be predicted from theory, it is still advisable to check the accuracy of a constructed device as an error can occur due to imperfect joints between the sheets of material that form the superconducting screen. The first step in such verification is to pass a test current through two windings of small and equal numbers of turns connected in series-opposition and observe the signal from the SQUID. Any measured output can then be expressed as a relative CCC error by dividing the output by that generated by a smaller test current in a single winding. A test conducted with windings of a small number of turns is the most stringent because the geometrical factor a/r_0 is not randomised and any breakthrough of flux between the connecting cables to the CCC and the SQUID is at its maximum effect. If a CCC has a sufficiently small error for a small number of turns, then it is likely that turns of larger number will have an even lower error. However, if desired, this can be verified by a binary build-up procedure where two windings of equal numbers of turns are connected in series and compared with a winding of twice the number of turns and so on.

4 Applications

4.1 Resistive dividers for voltage scaling

The first use of a CCC was to measure the ratio of cryogenic resistors configured as a voltage divider for scaling the voltage from a single Josephson junction at the mV level to a standard cell with an emf at the 1 V level [22]. The interconnections between the resistors were superconducting so as to provide a two-terminal measurement of the resistance ratio [23]. As illustrated in Fig. 7, this two-terminal measurement method only needs one detector as the current ratio is exactly equal to the resistor ratio.

The CCC is used to calibrate the ratio of the cryogenic resistors in situ. The circuit in Fig. 7 is shown configured for the resistance ratio measurement with the SQUID indicating the deviation of the resistor ratio R_X/R_Y from the 1:10 ratio of the CCC. To scale the 1 mV from the Josephson junction to 1 V, a final resistance ratio of 1000:1 is required, so three ratios of R_X/R_Y are measured: 0.1–1 Ω, 1–10 Ω and 10–100 Ω. For the voltage scaling, the switch in the circuit is configured so that the two arrows move to the left, connecting the 1 and 10 turn windings of the CCC in series as a null detector between the voltage across the Josephson junction and the voltage across R_X which has the value 0.1 Ω. The current flowing through R_X also flows through R_Y which has the value 1000 Ω so that a 1000:1 scaling is achieved. The power dissipation in the resistors for the ratio calibration and voltage scaling configurations is different so a series of small corrections has to be made for the resistor power coefficient, measured to be −0.013 ppm/mW.

A SQUID noise of $2.5 \times 10^{-4}\Phi_0$ rms for a 1 s average and a sensitivity for a single winding of 1.15 μA/Φ_0 were achieved. This translates to a current resolution of 0.3 nA rms and when the CCC is used as a null detector with 11 windings in series, this corresponds to 3 pV in 0.1 Ω. The total measurement uncertainty for the comparison of a standard cell with a Josephson junction using this approach was estimated to be 1.1 parts in 10^8, dominated by the determination of the power coefficient of the resistors. This method of relating the 1 mV output of a Josephson junction to the working unit level of a standard cell was the first practical application of a CCC for the scaling of an electrical quantity and represented an improvement of a factor of 10 over alternative methods at the time.

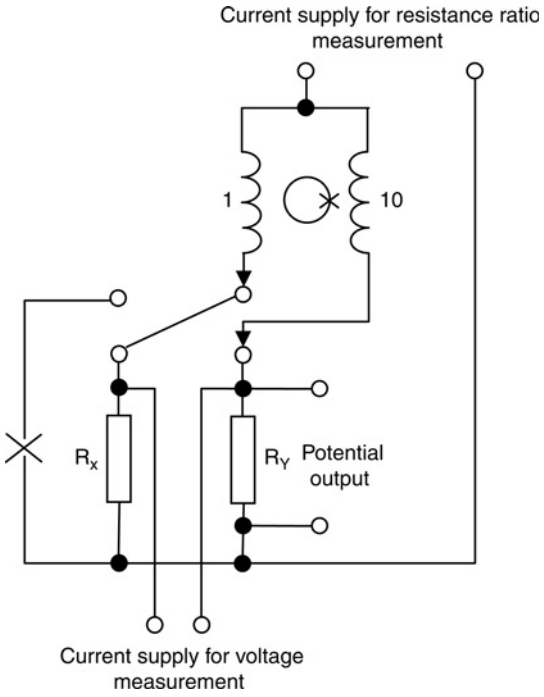

Fig. 7 *Two terminal resistance ratio bridge for voltage ratio*

In a later experiment, designed to relate the voltage of a 1 V Josephson junction array to a 10 V electronic Zener reference, an assessment of the power coefficient of the scaling resistors was made by configuring them as a 9:1 Hamon resistor network and measuring the power coefficient correction with a CCC under the same conditions of use as the voltage scaling measurement [24]. The overall uncertainty was again approximately one part in 10^8. It is an example of a four-terminal resistance ratio bridge using a CCC and this technique will now be described in more detail.

4.2 Four-terminal resistance measurement and the quantised Hall effect (QHE)

A natural extension of the use of the CCC for two-terminal cryogenic resistor measurement is the determination of four-terminal room temperature resistor ratios. Owing to the finite resistance of the connecting leads, the current no longer divides exactly according to the resistance ratio. The most common solution employed is to use two current sources [25] as illustrated in Fig. 8, which drive measurement currents through the resistor high and low-current terminals (H_C and L_C).

The bridge current is set by the primary current source and the slave current source is arranged to track the primary source with a constant of proportionality set as closely as possible to the reciprocal of the CCC winding ratio. Various methods have been developed to achieve the

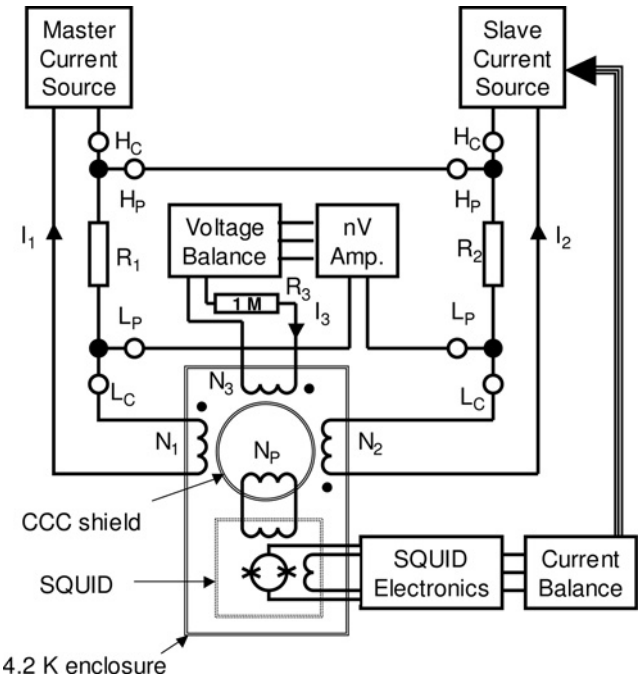

Fig. 8 *Schematic diagram of a general four-terminal CCC resistance ratio bridge*

necessary tracking using analogue or digital techniques [26–29]. Any remaining departure of the ratio N_1I_1/N_2I_2 generates a flux in the SQUID and this signal is used to correct the slave current in a negative feedback arrangement. The four-terminal measurement is completed by joining the two high potential terminals (H_P) together and measuring the voltage difference between the low potential terminals (L_P) with a sensitive detector.

The electrical isolation of the two bridge halves from each other and from the overall conducting screen surrounding the electronics is crucial to the overall accuracy of the bridge. The effect of leakage paths indicated by R_a to R_g in Fig. 9 needs to be considered carefully [30]. Direct leakage across the resistors being measured is to be avoided as this produces an error of the order of R_{std}/R_{leak} where R_{std} is the resistor

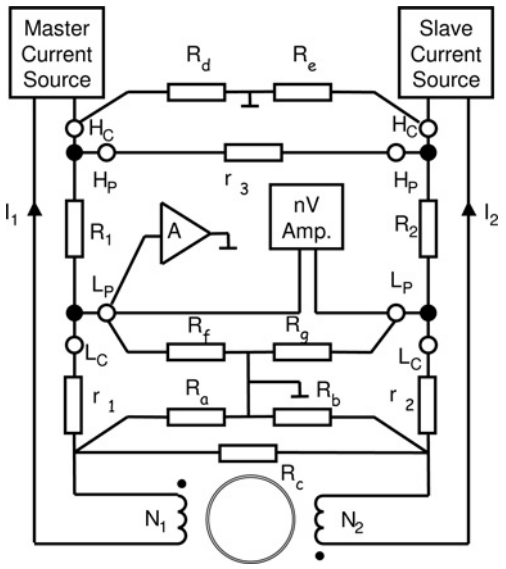

Fig. 9 *Illustration of the important current leakage paths in a CCC resistance ratio bridge*

being measured across which R_{leak} appears [31]. For leakage paths between the two halves of the bridge, if the voltage null detector is assumed to be balanced, then the only path of importance is R_C. The effect of a leakage here, close to the CCC windings, scales with bridge ratio [32] and is of the order of $N_1r_2/(N_2R_{leak})$ for $N_1 \gg N_2$ and $N_2r_1/(N_1R_{leak})$ for $N_2 \gg N_1$, with the errors in the two cases having opposite sign. For example, if the lead resistance were 1 Ω and the bridge ratio is 100:1, then the R_{leak} should be greater than 10^{11} Ω for an error of less than one part in 10^9. The rest of the leakage paths are between points on the measurement circuit and the conducting screen surrounding it. The effect of these leakage resistances on the measurement result depends on the potential between the circuit and the screen. If point L_P at R_1 is directly connected to the measurement screen, as in [32], then errors of the order R_1/R_{leak} for leakages R_d and R_e occur and this can only be minimised by ensuring that R_1 has the lower value of the two resistors being measured. The only arrangement that reduces all errors to the level r_{lead}/R_{leak} is for the potential difference between the L_P terminals and the screen to be maintained at zero using a high impedance buffer amplifier [26]. This result is independent of the measured resistance values and the bridge ratio. For a lead resistance of 1 Ω, a leakage resistance of greater than 10^9 Ω is required for an error of less than one part in 10^9. It should be noted that the position of the voltage null detector is also important. If it is placed at the H_P terminals instead, then the bridge is once more exposed to errors of the order of R_{std}/R_{leak}.

The voltage null detector output is normally brought close to zero by injecting a balance current in an auxiliary winding on the CCC. This can be done using a separately calibrated potential divider system [25, 32], or by a self-balancing feedback loop with a resistor of known value [8, 26, 33]. The accuracy required for this balance system depends on the deviation of the resistance ratio from nominal. High quality standard resistors are normally within one part in 10^5 of their nominal value and certainly not worse than one part in 10^4. For an overall ratio accuracy of one part in 10^9 in the case of a one part in 10^4 deviation, a relative accuracy of one part in 10^5 on the balance system is required.

The discovery of the QHE [34] gave an extra emphasis to the use of a CCC for resistance ratio measurement. The quantised resistance values follow the series $R = R_K/i$ where i is an integer and R_K is the von Klitzing constant. The most commonly used integers are $i = 2$ and $i = 4$ which, together with the internationally agreed value of R_K adopted since 1990, R_{K-90} [35], yield resistance values of 12.9064035 and 6.45320175 kΩ. The challenge placed on the designer of a CCC is to find a ratio of two integers which is close to the ratio of these quantised values to a decade resistance value and to have a total number of turns compatible with the required current sensitivity. An example ratio pair is 2065/16 and 2065/32 for the scaling of $i = 2$ and $i = 4$ values to 100 Ω, respectively [36] and these differ from the desired ratio by only 11.89346×10^{-6} which is well within the measurement range of a typical CCC ratio bridge. Bridges based on a CCC for measurements of the QHE were rapidly brought into operation [32, 37, 38] and measurements close to the theoretical noise limit were demonstrated using a second SQUID with matching transformer as the voltage null detector [39]. CCC ratio bridges are now used by many National Metrology Institutes around the world to maintain their local resistance standards. Comparison between

doi: 10.1049/iet-smt.2010.0170

systems using travelling resistance standards normally demonstrates equivalence at the level of a few parts in 10^8 or better, the performance frequently being limited by the stability of the resistance standards [40].

For room temperature resistance measurements, it is possible to design a CCC bridge so that all noise components are less than the Johnson noise in the resistors being measured. Under these conditions, the resolution (defined here as the ratio of the noise voltage to the bridge voltage) depends only on the bridge ratio and the measurement power dissipation, not on the absolute value of the resistors being measured. In a current comparator bridge, the smaller resistor dissipates the larger power so this sets the maximum measurement voltage or current, typically in the range 1 to 10 mW. The Johnson noise power in any resistor for a 1 Hz bandwidth is $P_n = 4k_BT = 1.6 \times 10^{-20}$ W at 293 K, where k_B is the Boltzmann constant. The noise power seen by the null detector in the bridge is the sum of the powers in the two resistors, so for a 1:α ratio measurement the voltage noise at the detector will be $V_n^2 = P_n(1 + \alpha)R$ where R is the smaller resistor. Thus for a power dissipation in the smaller resistor of P_m, the resolution will be $\sqrt{P_n(1 + \alpha)/P_m}$ and for $\alpha = 10$ this corresponds to 1.3 parts in 10^8 for $P_m = 1$ mW.

The bridge electronics should be designed so that there is sufficient gain in the SQUID feedback loop that the noise from the current sources is reduced below that of the CCC and SQUID combination [30]. The noise contributions are then the CCC–SQUID noise and the voltage and current noise of the voltage null detector. Fig. 10 shows the voltage and current noise components of a high quality null detector together with the Johnson noise from the resistors being measured. In this example, the values used are 1 nV$\sqrt{\text{Hz}}$ and 0.5 pA$\sqrt{\text{Hz}}$. It can be seen that the Johnson noise of the room temperature resistors dominates over the resistance range 15 Ω to 15 kΩ, so this detector is suitable for 10:1 ratio measurements over the range 1 Ω to 10 kΩ. However, for a QHR measurement to 100 Ω, the QHR, being at 0.3 K, has a lower Johnson noise than the 100 Ω resistor so the critical component becomes the current noise of the null detector with a value of 0.1 pA/$\sqrt{\text{Hz}}$ being required for this not to dominate. A lower current noise detector can be made using a SQUID with appropriate flux

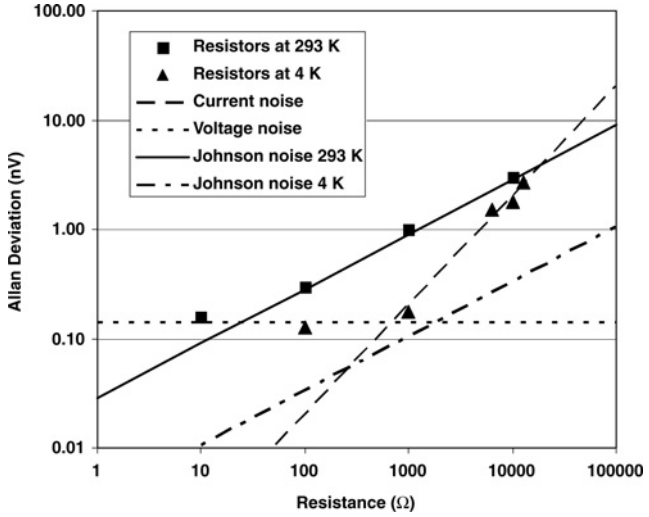

Fig. 10 *Noise of a null detector for a range of source resistances, expressed as an Allan deviation for a 10 s measurement interval*

transformer [39]. The current noise due to the CCC–SQUID combination must also be below this level. For a typical number of turns of 2065 and CCC sensitivity of 5 μA/Φ_0 for a single turn, a SQUID noise of better than 4×10^{-5} $\Phi_0/\sqrt{\text{Hz}}$ is required.

A CCC ratio bridge is the ideal tool for comparing one QHR sample with another. A specially constructed bridge was used to demonstrate the universality of the QHR to a relative uncertainty of three parts in 10^{10} by comparing the $i = 2$ plateau in a GaAs/AlGaAs heterostructure with the $i = 4$ plateau in a silicon metal–oxide semiconductor field-effect transistor (MOSFET) [41]. Further investigations of material and plateau independence of the QHE showed no significant effect at a similar level of uncertainty [42]. The CCC played a key role in the measurements of R_K in SI units where it formed part of a long measurement chain from a QHE sample measured with direct current, via a resistor with calculable difference between direct and alternating current, to a capacitor with calculable value in terms of the permittivity of free space, ε_0. With the assumption that R_K is exactly equal to the ratio h/e^2, where h is the Planck constant and e is the charge on an electron, this measurement makes an important contribution to the determination of the fundamental physical constants [43, 44].

A CCC ratio bridge can also be used to verify other ratio standards, designed to be accurate from first principles. An example is a resistance network designed for verifying the linearity of resistance thermometry bridges where four resistors can be selected in different combinations to give 35 different resistance values all related by the formulae for series and parallel connection of resistors [45]. Verification of the network performance with a CCC bridge demonstrated consistency with the calculated values at the $n\Omega/\Omega$ level.

4.3 Low-value resistors

The CCC applications described so far have typically used a CCC with a flux linkage in the region of 0.1 A in a single turn. For the measurement of resistors below 1 Ω, currents above 0.1 A are required and measurements up to 100 A are common on higher power resistors and shunts. A CCC and associated resistance bridge has been developed specially for this resistance range [46]. The flux linkage for a single turn at 100 A is 1000-fold larger than normally encountered and this introduces two design challenges. First of all, the SQUID null detector is much too sensitive with the result that the peak-to-peak noise on even the best 100 A current sources will be many times a flux quantum. This problem was solved by connecting a short length of superconducting wire across the SQUID input terminals. This attenuates the signal in the SQUID by the ratio of its inductance to the SQUID input coil inductance in parallel with the CCC pickup coil. The basic sensitivity of the CCC for a single turn of 13 μA/Φ_0 was reduced by a factor of nearly 1000 to 10 mA/Φ_0. Secondly, the local field generated by a single conductor carrying 100 A might drive a superconducting shield normal since the field close to a 1 mm diameter wire carrying 100 A is 0.05 T compared to the critical field of lead, for example, which is 0.08 T. This problem is reduced by using a Type II CCC so that the current-carrying wires can be located some distance away from any of the superconducting screens. A test of the CCC ratio accuracy on a 1000:1000 ratio, wound with superconducting wire, up to a flux linkage of 1000 A turns revealed no error within the measurement resolution of one part in 10^9. However,

a test of the 1:1 ratio, which was constructed using copper wire, revealed a change in the SQUID output corresponding to several parts in 10^8 when the current was increased from zero to 100 A. This change was independent of current direction and so was attributed to a temperature increase in the helium bath due to heat dissipation in the winding rather than a ratio error. This effect therefore does not lead directly to an error on a measured resistor ratio but does contribute to the Type A uncertainty components. (A Type A evaluation of a standard uncertainty is an estimate for a quantity that varies randomly, whereas a Type B evaluation is not based on repeated observations but is instead evaluated by scientific judgement [47].)

The Type A uncertainty achieved for low power measurements, in the range 1–10 mW, is limited in this design by the noise of the voltage null detector corresponding to the equivalent Johnson noise in a resistor of approximately 1 Ω. Nevertheless, uncertainties ranging from 0.03 μΩ/Ω for a 0.1 Ω resistor measured at 1 mW to 0.2 μΩ/Ω for a 100 μΩ resistor measured at 10 mW were achieved. The Type A uncertainty for high power measurements becomes dominated by the stability of the resistor under test. As an example, an uncertainty of a few parts in 10^7 was achieved for a 10 mΩ resistor measured at currents up to 50 A. In addition to resistor ratio measurement of low ohmic resistors, a high current CCC can also be used to verify the ratio accuracy of room-temperature current comparators based on magnetic shields and detection cores. In this application, the uncertainty will be limited only by the properties of the comparators being compared as no resistors are involved.

4.4 High-value resistors and small currents

At the other end of the scale from high current measurement, the CCC has also been extensively explored for the measurement of high value resistors and small currents. Here the motivation is to combine the high ratio accuracy of a CCC with as high a current resolution as possible.

The first application of a CCC to high resistance measurement was for resistors up to 1 MΩ and used a CCC originally designed for QHR measurements, where the largest winding available had 1600 turns [48]. The quoted sensitivity was 700 pA/√Hz for a single turn leading to a value for 1600 turns of 440 fA/√Hz, which is about the same as the current noise of the null detector used in the bridge so that the total current noise is about a factor of √2 worse. The current noise due to Johnson noise in a 1 MΩ resistor is 13 fA/√Hz so the noise in the measurement is dominated by the SQUID and null detector. For a measurement of 10 kΩ to 1 MΩ at a bridge voltage of 5 V as used by the authors, the current noise sets a resolution of approximately 1.5×10^{-7} in a 1 Hz bandwidth. A Type A uncertainty of 8×10^{-9} was achieved for a 10 kΩ to 1 MΩ ratio but the overall accuracy of the measurement was limited to 5×10^{-8} by Type B uncertainties due to leakage currents.

An increased number of turns gives more sensitivity as demonstrated in a CCC resistance ratio bridge for comparing a 100 MΩ resistor directly with a QHE sample [49]. Here a two-terminal CCC bridge with a single energising source (Fig. 7) was used and connection to the devices was made by adopting a cryogenic resistor and a special property of QHR devices whereby an accurate two-terminal definition can be realised remotely from the device using a multiple-series connection [50]. The CCC sensitivity quoted for a single turn is 170 pA/√Hz and this leads to a sensitivity for a 15 500 turn winding of 11 fA/√Hz, an improvement of a factor of 40 on the previous figure above. A separate null detector is not needed in a two-terminal configuration so there is no extra noise from this component. The current noise from the 100 MΩ resistor at 4.2 K is 1.5 fA/√Hz. It is important to note that the sensitivity quoted is for a complete measurement system, including all connecting cables and the extra noise observed over that theoretically obtainable is attributed to the induced voltages caused, for example, by vibration of leads in the magnetic field of the QHR system. The maximum current that could be handled by the QHR device of 73 μA in turn limited the current in the 100 MΩ resistor to about 10 nA so the measurement resolution was approximately one part in 10^6 for a 1 Hz bandwidth. A large number of turns on a CCC can result in a resonance at audio frequencies which, if left undamped, can give rise to instability in the SQUID control loop. Here damping was provided by using resistive wire for the large winding, and other researchers have also included resistive foil screens in the design to increase the damping further [51].

In the measurement of high value resistors, the resistance of the connecting leads is a smaller fraction of the resistors under test. If the lead resistances are not negligible, then they can be measured and a correction made [52]. Alternatively, a four-terminal measurement can be realised as illustrated in Fig. 11. Here the current division ratio is set by adjusting resistor R_A so as to achieve a minimum SQUID signal and the deviation of the resistor ratio R_1/R_2 is indicated by the voltage detector. A resistor network consisting of r_1 and r_2 is used to reduce the effect of resistance in the connecting leads and it can be easily shown that the residual error in the resistor ratio R_1/R_2 can be approximated by

$$\varepsilon \simeq \frac{rr_1}{(r + r_1 + r_2)R_1}\left(\frac{R_1 r_2}{R_2 r_1} - 1\right)$$

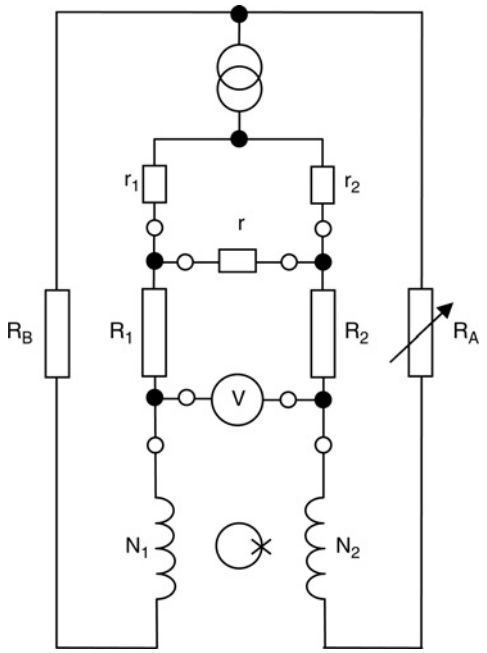

Fig. 11 *Schematic diagram of a four-terminal bridge employing a resistance network to reduce the effect of voltage drop in the connecting leads*

doi: 10.1049/iet-smt.2010.0170

where r is the resistance of the connection between the potential terminals of the two resistors being compared. Thus, if the ratio R_1r_2/R_2r_1 is chosen to be within one part in 10^4 of unity and r/R_1 is less than 10^{-4} then the error will be less than one part in 10^8. This arrangement is practical for resistance values of 10 kΩ or higher with lead resistances of 1 Ω or less and fixed components can be used avoiding the need for a secondary bridge balance adjustment. This circuit configuration requires a voltage detector but this component can be satisfied by a low current noise operational amplifier. Commercial components with a current noise of 10 fA p–p in a 0.1–10 Hz bandwidth are available which is comparable with the equivalent current noise of the CCC.

The advent of single electron transport devices, with the promise of providing a quantum standard of current, has introduced another potentially key role for the CCC. Here the challenge is to relate the current from such a device (electron charge × frequency) to the established quantum standards of voltage and resistance [53]. This task has been known as the closure of the 'metrological triangle' [54]. Systems have been developed using a CCC with a large turns ratio (greater than 10:000 to 1) so as to scale the small current from a single electron device to a larger current which can then be passed through a resistor [55] or directly through a QHR device [56]. In a practical system, the maximum resolution set by the SQUID intrinsic noise is often degraded by extra noise sources such as trapped magnetic flux in the CCC and noise currents from microphonics in the connecting cables. The performance of four CCCs optimised for small current measurement is summarised in Table 2 with figures given for both the theoretical maximum current resolution and what was measured in practice. Undesirable effects due to connecting leads can be reduced by placing the CCC in the same cryogenic environment as the single electron transport device with resolutions achieved of 50 aA for a 1 h measurement using a test current [57] and 12 aA for a 12 h measurement of a single electron device producing a current of a few pA [58].

4.5 Alternating current ratio

A CCC can also be used for measuring the ratio of alternating currents. A device constructed in the manner normally used for direct current has a significant frequency-dependent error due to combination of the series inductance of the windings and their parallel capacitance. The measured current ratio has an in-phase error of the form $(1 - k)\omega^2 LC$, where k is the coupling between the two windings and L and C are the series inductance and parallel capacitance of a winding, respectively. Typical values of $(1 - k)L = 4$ mH and $C = 800$ pF led to an estimated error at 4 Hz of about two parts in 10^9 [59]. A resistance ratio bridge based on a CCC with alternating current is more complex than the corresponding design for direct current as additional care has to be taken over currents which flow in stray capacitances. Furthermore, it is difficult to obtain a high loop gain in the SQUID feedback system at the measurement frequency. Overall bridge accuracy is therefore ensured by careful matching of the primary and secondary current sources in the bridge and as high a loop gain as possible [60, 61]. An advantage of low-frequency alternating current for resistance ratio measurements is that $1/f$ noise sources in the measurement system, such as in the SQUID null detector, can be avoided. Low-frequency measurements can also be used to explore the ac/dc difference of resistors in the 0.1–1 Hz frequency range. These can be caused by dielectric losses or the Peltier effect and can be as large as one part in 10^7 [60].

The performance of a CCC with alternating current can be significantly enhanced if steps are taken to reduce the effect of the stray capacitance. Auxiliary wound cores can be added to the design in order to null the alternating voltage developed across the CCC windings [62, 63]. One core is required for each active winding and their energisation has to be separately adjusted until the measured voltage across each of the windings is null. This compensation reduces the effect of capacitance between individual turns. In a separate step, the effect of capacitance between the winding and its surroundings is compensated by a variable shunt capacitance connected across the winding input. This can be done as a self-calibration procedure by using coaxial cable for the windings and using the outer shield as a return path for the current during the adjustment of the trim capacitor. Correct adjustment is indicated by zero signal on the CCC null detector. A comparator correctly adjusted in this manner can then have ratio errors as low as one part in 10^8 at frequencies up to 10 kHz, compared with an uncompensated design which would have errors of the order of 1% at these frequencies.

An alternative approach for achieving a high-frequency performance is to use thin film fabrication techniques to form a CCC [64]. Here a planar construction is used to fabricate coils with a self-resonance frequency in the 100 MHz region suggesting that frequency-dependent errors would be less than one part in 10^8 up to 10 kHz. However, prototypes constructed with this technique had a ratio error at dc, due to geometry, of the order of 500 parts in 10^6 and this would need to be calibrated and remain stable for a practical ac device to be realised.

Table 2 Summary of CCC designs for low current measurement giving details of the SQUID noise, CCC sensitivity for a single turn, number of turns employed, theoretical maximum resolution and the resolution obtained in practice

Author	Intrinsic SQUID noise $\mu\Phi_0/\sqrt{\text{Hz}}$	CCC sensitivity $\mu\text{A}/\Phi_0$ (1 turn)	Turns	Max. resolution fA/$\sqrt{\text{Hz}}$	Claimed resolution fA/$\sqrt{\text{Hz}}$
Gay *et al.* [55]	5.7	5.0	10 000	2.9	4.0
Rietveld *et al.* [16]	11	2.3	30 000	0.8	2.1
Elmquist *et al.* [49]	5.0	3.8	15 500	1.2	11
Janssen and Hartland [56]	3.2	10.7	40 960	0.5	6

5 New materials and special designs

The availability of materials which are superconducting at the boiling point of liquid nitrogen, 77 K, gives scope to make a cryogenic current comparator operating at this temperature. However, unlike the thin, malleable Pb-alloy foil used to provide the coaxial shielding in most CCCs for operation at 4.2 K, high temperature superconductor (HTS) materials are ceramics and are produced in particular shapes that cannot

be easily modified afterwards. One approach is to use long tubes fabricated in HTS materials such as $YBa_2Cu_3O_7$ (YBCO) and $Ba_2Sr_2CaCu_3O_8$ (BSCCO). A simple design is to use two parallel tubes, 100 mm in length, with an HTS-SQUID mounted in the gap between them [65]. The CCC windings pass through the tubes and it was found in this example that the current-linkage error decreased away from the tube ends and changed sign at the half-way point. The error varied approximately linearly from -2×10^{-5} to 2×10^{-5} over a distance of -10 mm to $+10$ mm about the centre. This design had a sensitivity of 270 $\mu A/\Phi_0$ for a single turn and the SQUID noise was $2.5 \times 10^{-4}\ \Phi_0/\sqrt{Hz}$, giving a corresponding current resolution for a single turn of 25 $nA/\sqrt{Hz}$. Other approaches using bulk materials include components machined from YBCO and assembled to form the geometry of a Type-I CCC, prototypes of this design achieving ratio errors of parts in 10^4 [66], also cylinders of MgB_2 with a machined U-shaped coil recess [67].

As an alternative to bulk materials, thick films coated onto a substrate can also be used to construct CCC tubes. A prototype has been successfully constructed using $Tl_2Ba_2Ca_2Cu_3O_x$ (Tl-2223) coated on both the inner and outer surfaces of MgO tubes [68]. Four parallel tubes were used to construct the CCC with a winding in each pair as illustrated in Fig. 12. In one design the tubes were spaced by insulators and in another, pairs of shields carrying the windings in the same direction were joined along their length by a superconducting joint. In principle, no flux would pass between these shields in the region of the joint when the windings carry equal current, but the superconducting joint is included to reduce any non-ideal behaviour and thereby improve the accuracy and stability of the device.

The tubes were 200 mm long and 10 mm diameter and were spaced to give a 4 mm aperture for the SQUID which is located in the central region. The ratio error was tested up to 2 A turns and found to be exponentially decreasing as the SQUID was moved from the tube ends towards the centre where it fell below 1×10^{-6}. The version with the joined tubes showed a nearly constant error of order 1×10^{-6} over a central region of ± 20 mm. Although the accuracy of this design is improved over the design with bulk tubes, the sensitivity is reduced to 1740 $\mu A/\Phi_0$ for the insulated tube version and sensitivity of 2460 $\mu A/\Phi_0$ for the joined tube version. This corresponds to resolutions of 440 and 620 $nA/\sqrt{Hz}$, respectively, for a SQUID noise of $2.5 \times 10^{-4}\ \Phi_0/\sqrt{Hz}$. The reduced sensitivity is attributed to the fact that only 0.2% of the flux passing through the aperture is sensed by the SQUID.

In HTS CCC designs, the lack of suitably flexible wires and materials that can be reliably joined while maintaining a superconducting connection means that flux transformers to optimise the coupling of the CCC to the SQUID cannot be constructed. However, the coupling of the CCC to the SQUID can be improved by using a flux concentrator [69]. Here advantage is taken of the thin film HTS coating on a substrate in that a gap can be introduced into the outer layer and the gap bridged at just one place forcing the current to flow through one place. The motivation for this design was to make a CCC based on HTS materials for measuring ion beam currents. The field profile generated by the bridge is very well suited to detection by a SQUID gradiometer. There are two limits to the design of the bridge. First, the cross-section must not be so small that the critical current density of the superconducting film is exceeded and secondly, the inductance of the bridge must be less than the alternative current path via the underlying surfaces of the superconducting film [70]. Calculation and measurement of the field gradient produced by a simple 12 mm × 4 mm bridge gives $\sim 1\ \mu T\ cm^{-1}$ for a current of 7 mA. If this is efficiently coupled to a gradiometer with typical sensitivity of 0.1 $pT\ cm^{-1}\ Hz^{-1/2}$, then an equivalent current noise of better than 1 $nAHz^{-1/2}$ is possible. More complex bridge structures, such as a double loop, can be fabricated to improve the coupling to a gradiometer [71]. For a tube length of 100 mm, the error in the CCC, for two equal currents, was observed to be 1×10^{-3}. The resolution was estimated to be 4 nA $Hz^{-1/2}$.

An HTS CCC for ion beam measurement has been successfully integrated with a closed cycle cooler [72]. The system was tested against a Faraday cup monitor for beam currents of 600 nA and 7 μA and showed a basic resolution of 400 nA.

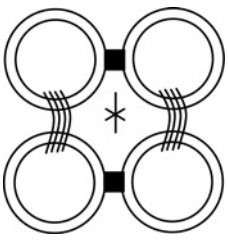

Fig. 12 *Cross-section of HTS comparator showing four cylinders and the location of the windings and planar SQUID sensor*

6 Summary

The CCC has played a key role in electrical metrology over the last 40 years and its very high ratio accuracy of better than one part in 10^9 and high current sensitivity means that it is the ideal component for scaling the voltage, resistance or current from a Josephson, QHE or single electron transport device, respectively, to practical working values. As each of these electrical quantum effects emerged, the CCC was rapidly deployed in order to make the most accurate measurements in the established SI system. The theory of the sensitivity and accuracy of a CCC is now well understood; so it is possible for researchers to make devices to well-established principles and formulae. The CCC has been successfully deployed in measurement systems for the routine calibration of electrical standards, and QHE primary resistance standards based on a CCC bridge have been commercially available for over 15 years.

Although the majority of routinely operating devices are based on materials that are superconducting below 10 K, requiring liquid helium cooling, considerable effort has been invested in designs based on HTS materials. These have yet to achieve the combination of accuracy and sensitivity enjoyed by their lower temperature counterparts but the potential for operation at 77 K is sufficiently attractive for research to continue. The independence of the CCC accuracy from the geometry of the ratio windings has been used to advantage outside electrical metrology for the measurement of ion beam currents, where insensitivity to the position of the beam as it passes through the measurement device is required.

The challenge placed on a CCC to scale the current from a single-electron transport device so that it can be measured in terms of the Josephson effect and QHE in the metrological triangle to a sufficient accuracy still has to be met. It is

doi: 10.1049/iet-smt.2010.0170

estimated that closure of the metrological triangle with an uncertainty approaching one part in 10^8 is required in order to influence the least squares adjustment of the fundamental constants based on existing experimental data [73]. In order to meet this target, an operating current in the nA to μA range from single-electron transport devices is almost certainly required since, as has been shown, the current resolution of a practical CCC is limited to the order of 10 aA.

7 Acknowledgments

The author is grateful to Gert Rietveld for his contribution to the original planning and scope of this review and to John Gallop for his critical review of the manuscript.

8 References

1 Fagaly, R.L.: 'Superconducting quantum interference device instruments and applications', *Rev. Sci. Instrum.*, 2006, **77**, p. 101101
2 Hartland, A.: 'Quantum standards for electrical units', *Contemp. Phys.*, 1988, **29**, p. 477
3 Jeckelmann, B., Jeanneret, B.: 'The quantum Hall effect as an electrical resistance standard', *Rep. Progr. Phys.*, 2001, **64**, pp. 1603–1655
4 Gallop, J., Piquemal, F.: 'SQUIDs for standards and metrology', in Clarke, J., Braginski, A. (Eds.): 'The SQUID handbook: applications of SQUIDs and SQUID systems' (Wiley, 2006, vol. II), Ch. 9
5 Harvey, I.K.: 'A precise low temperature dc ratio transformer', *Rev. Sci. Instrum.*, 1972, **43**, (11), pp. 1626–1629
6 Sullivan, D.B., Dzuiba, R.F.: 'Low temperature direct current comparators', *Rev. Sci. Instrum.*, 1974, **45**, (4), pp. 517–519
7 Grohmann, K., Hahlbohm, H.D., Lübbig, H., Ramin, H.: 'Ironless cryogenic current comparators for AC and DC applications', *IEEE Trans. Instrum. Meas.*, 1974, **IM-23**, (4), pp. 261–263
8 Williams, J.M., Janssen, T.J.B.M., Rietveld, G., Houtzager, E.: 'An automated cryogenic current comparator resistance ratio bridge for routine resistance measurements', *Metrologia*, 2010, **47**, pp. 167–174
9 Witt, T.J., Reymann, D.: 'Using power spectra and Allan variances to characterise the noise of Zener-diode voltage standards', *IEE Proc. Sci. Meas. Technol.*, 2000, **147**, pp. 177–182
10 van der Wel, W., Mooij, J.E., Harmans, C.J.P.M.: 'Cryogenic current comparator with increased resolution', *Rev. Sci. Instrum.*, 1988, **59**, (4), pp. 624–626
11 Symm, G.T.: 'Design of a cryogenic current comparator', in Brebbia, C.A., Dominguez, J., Paris, F. (Eds.): 'Proc. boundary elements XIV: field problems and applications', vol. 11992, pp. 519–526
12 Sese, J., Lera, F., Camon, A., Rillo, C.: 'Calculation of effective inductances of superconducting devices – application to the cryogenic current comparator', *IEEE Trans. Appl. Superconduct.*, 1999, **9**, (1), pp. 58–62
13 Early, M.D., Jones, K.: 'Optimum sensitivity of an externally shielded cryogenic current comparator', *IEEE Trans. Instrum. Meas.*, 1997, **46**, (6), pp. 459–462
14 Sese, J., Bartolome, E., Camon, A., Flokstra, J., Rietveld, G., Rillo, C.: 'Simplified calculus for the design of a cryogenic current comparator', *IEEE Trans. Instrum. Meas.*, 2003, **52**, (2), pp. 612–616
15 Early, M.D., van Dam, M.A.: 'Results from a detailed calculation of the sensitivity of a cryogenic current comparator', *IEEE Trans. Instrum. Meas.*, 1999, **48**, (2), pp. 379–382
16 Rietveld, G., Bartolomé, E., Sesé, J., *et al.*: '1:30 000 cryogenic current comparator with optimum SQUID readout', *IEEE Trans. Instrum. Meas.*, 2003, **52**, (2), pp. 621–625
17 Grohmann, K., Hahlbohm, H.D., Hechtfisher, D.: 'The cryo current comparator as a calculable DC ratio standard', *IEEE Trans. Instrum. Meas.*, 1979, **IM-28**, (3), pp. 205–211
18 Bridge, J.F., Angrist, S.W.: 'An extended table of roots of $J'_n(x)Y'_n(\beta x) - J'_n(\beta x)Y'_n(x) = 0$', *Math. Comput.*, 1962, **16**, pp. 198–204
19 Grohmann, K., Hahlbohm, H.D., Hechtfisher, D., Lübbig, H.: 'Field attenuation as the underlying principle of cryo current comparators', *Cryogenics*, 1976, **16**, (7), pp. 423–429
20 Seppa, H.: 'The ratio error of the overlapped-tube cryogenic current comparator', *IEEE Trans. Instrum. Meas.*, 1990, **39**, (5), pp. 689–697
21 Grohmann, K., Hahlbohm, H.D., Hechtfischer, D., Lübbig, H.: 'Field attenuation as the underlying principle of cryo-current comparators 2. Ring cavity elements', *Cryogenics*, 1976, **16**, (10), pp. 601–605
22 Sullivan, D.B., Dziuba, R.F.: 'A low-temperature direct-current comparator bridge', *IEEE Trans. Instrum. Meas.*, 1974, **IM-23**, (4), pp. 256–260
23 Harvey, I.K.: 'Cryogenic ac Josephson effect emf standard using a superconducting current comparator', *Metrologia*, 1976, **12**, pp. 47–54
24 Henderson, L.C.A., Hartland, A., Williams, J.M.: 'Measurements of 10 V standards using a 1 V Josephson array', *IEEE Trans. Instrum. Meas.*, 1993, **42**, (2), pp. 577–579
25 Delahaye, F.: 'A double constant current source for cryogenic current comparators and its applications', *IEEE Trans. Instrum. Meas.*, 1978, **IM-27**, (2), pp. 426–429
26 Williams, J.M., Hartland, A.: 'An automated cryogenic current comparator resistance ratio bridge', *IEEE Trans. Instrum. Meas.*, 1991, **40**, (2), pp. 267–270
27 Elmquist, R.E., Dziuba, R.F.: 'Isolated ramping current sources for a cryogenic current comparator bridge', *Rev. Sci. Instrum.*, 1991, **62**, (10), pp. 2457–2460
28 Götz, M., Drung, D., Pesel, E., *et al.*: 'Improved cryogenic current comparator setup with digital current sources', *IEEE Trans. Instrum. Meas.*, 2009, **58**, (4), pp. 1176–1182
29 Sanchez, C.A., Wood, B.M., Inglis, A.D.: 'CCC bridge with digitally controlled current sources', *IEEE Trans. Instrum. Meas.*, 2009, **58**, (4), pp. 1202–1205
30 Williams, J.M., Rietveld, G., Houtzager, E., Janssen, T.J.B.M.: 'Design considerations for a CCC bridge with complete digital control', *IEEE Trans. Instrum. Meas.*, doi: 10:1109/TIM.2011.2149330, 2nd June 2011
31 Elmquist, R.E.: 'Leakage current detection in cryogenic current comparator bridges', *IEEE Trans. Instrum. Meas.*, 1993, **42**, pp. 167–169
32 vander Wel, W., Mooij, J.E., Harmans, C.J.P.M., *et al.*: 'A resistance ratio bridge based on a cryogenic current comparator for measuring the quantized Hall resistance', *IEEE Trans. Instrum. Meas.*, 1989, **38**, (1), pp. 54–58
33 Kinoshita, J., Inagaki, K., Yamanouchi, C., *et al.*: 'Self-balancing resistance ratio bridge using a cryogenic current comparator', *IEEE Trans. Instrum. Meas.*, 1989, **38**, (2), pp. 290–292
34 von Klitzing, K., Dorda, G., Pepper, M.: 'New method for high accuracy determination of the five structure constant based on quantized Hall resistance', *Phys. Rev. Lett.*, 1980, **45**, pp. 494–497
35 Petley, B.W.: 'The role of the fundamental constants of physics in metrology', *Metrologia*, 1992, **29**, pp. 95–112
36 Delahaye, F., Reymann, D.: 'Progress in resistance ratio measurements using a cryogenic current comparator at LCIE', *IEEE Trans. Instrum. Meas.*, 1985, **Im-34**, (2), pp. 316–319
37 Hartland, A.: 'Use of a cryogenic current comparator to determine the quantized Hall resistance in a silicon MOSFET'. Proc. Precision Meas. Fund. Constants II, NBS Special Publication, 1982, vol. 617, pp. 543–548
38 Jeckelmann, B., Fasel, W., Jeanneret, B.: 'Improvements in the realization of the quantized Hall resistance standard at OFMET', *IEEE Trans. Instrum. Meas.*, 1995, **44**, pp. 265–268
39 Delahaye, F., Bournaud, D.: 'Low-noise measurements of the quantized Hall resistance using an improved cryogenic current comparator bridge', *IEEE Trans. Instrum. Meas.*, 1991, **40**, (2), pp. 237–240
40 Nakanishi, M., Kinoshita, J., Endo, T., *et al.*: 'Comparison of resistance standards between the National Institute of Metrology (China) and the Electrotechnical Laboratory (Japan)', *Metrologia*, 2002, **39**, pp. 207–212
41 Hartland, A., Jones, K., Williams, J.M., Gallagher, B.L., Galloway, T.: 'Direct comparison of the quantized Hall resistance in gallium-arsenide and silicon', *Phys. Rev. Lett.*, 1991, **66**, (8), pp. 969–973
42 Jeckelmann, B., Inglis, A.D., Jeanneret, B.: 'Material, device and step independence of the quantized Hall resistance', *IEEE Trans. Instrum. Meas.*, 1995, **44**, (2), pp. 269–275
43 Hartland, A., Jones, R.G., Kibble, B.P., Legg, D.J.: 'The relationship between the SI ohm, the ohm at NPL and the quantized Hall resistance', *IEEE Trans. Instrum. Meas.*, 1987, **IM-36**, (2), pp. 208–213
44 Jeffery, A., Elmquist, R.E., Shields, J.Q., *et al.*: 'Determination of the von Klitzing constant and the fine-structure constant through a comparison of the quantized Hall resistance and the ohm derived from the NIST calculable capacitor', *Metrologia*, 1998, **35**, pp. 83–96
45 White, D.R., Williams, J.M.: 'Resistance network for verifying the accuracy of resistance bridges', *IEEE Trans. Instrum. Meas.*, 1997, **46**, (2), pp. 329–332
46 Williams, J.M., Kleinschmidt, P.: 'A cryogenic current comparator bridge for resistance measurements at currents of up to 100 A', *IEEE Trans. Instrum. Meas.*, 1999, **48**, (2), pp. 375–378
47 ISO/IEC Guide 98-3:2008: 'Uncertainty of measurement – Part 3: Guide to the expression of uncertainty in measurement' (GUM, 1995)

48 Pesel, E., Schumacher, B., Warnecke, P.: 'Resistance scaling up to 1 MΩ at PTB with a cryogenic current comparator', *IEEE Trans. Instrum. Meas.*, 1995, **44**, (2), pp. 273–275

49 Elmquist, R.E., Hourdakis, E., Jarrett, D.G., Zimmerman, N.M.: 'Direct resistance comparisons from the QHR to 100 MΩ using a cryogenic current comparator', *IEEE Trans. Instrum. Meas.*, 2005, **54**, (2), pp. 525–528

50 Delayhaye, F.: 'Series and parallel connection of multi-terminal quantum Hall effect devices', *J. Appl. Phys.*, 1993, **73**, pp. 7914–7920

51 Rietveld, G., de la Court, P., van den Brom, H.: 'Internally damped CCC for accurate measurements of small electrical currents', *IEEE Trans. Instrum. Meas.*, 2009, **58**, (4), pp. 1196–1201

52 Bierzychudek, M.E., Elquist, R.E.: 'Uncertainty evaluation in a two-terminal cryogenic current comparator', *IEEE Trans. Instrum. Meas.*, 2009, **58**, (4), pp. 1170–1175

53 Hartland, A.: 'The quantum Hall effect and resistance standards', *Metrologia*, 1992, **29**, pp. 175–190

54 Piquemal, F., Geneves, G.: 'An argument for a direct realization of the quantum metrological triangle', *Metrologia*, 2000, **37**, pp. 207–211

55 Gay, F., Piquemal, F., Geneves, G.: 'Ultralow noise current amplifier based on a cryogenic current comparator', *Rev. Sci. Instrum.*, 2000, **71**, (12), pp. 4592–4595

56 Janssen, T.J.B.M., Hartland, A.: 'Accurate measurement of currents generated by single electrons transported in a one-dimensional channel', *IEE Proc. Sci. Meas. Technol.*, 2000, **147**, (4), pp. 174–176

57 de Wilde, Y., Gay, F., Piquemal, F.P.M., Genevès, G.: 'Measurements of single electron transistor devices combined with a CCC: progress report', *IEEE Trans. Instrum. Meas.*, 2001, **50**, (2), pp. 231–234

58 Feltin, N., Devoille, L., Piquemal, F., Lotkhov, S.V., Zorin, A.B.: 'Progress in measurements of a single-electron pump by means of a CCC', *IEEE Trans. Instrum. Meas.*, 2003, **52**, (2), pp. 599–603

59 Delahaye, F.: 'An AC-bridge for low-frequency measurements of the quantized Hall resistance', *IEEE Trans. Instrum. Meas.*, 1991, **40**, (6), pp. 883–888

60 Seppa, H., Satrapinski, A., Varpula, T., Saari, J.M.: 'Frequency-dependence of 100-omega standard resistors measured with a CCC-based ac resistance bridge', *IEEE Trans. Instrum. Meas.*, 1995, **44**, (2), pp. 276–280

61 Seppa, H., Satrapinski, A.: 'AC resistance bridge based on the cryogenic current comparator', *IEEE Trans. Instrum. Meas.*, 1997, **46**, (2), pp. 463–466

62 Grohmann, K., Hechtfischer, D.: 'Self-calibrating cryo current comparators for AC applications', *IEEE Trans. Instrum. Meas.*, 1984, **IM-33**, (2), pp. 91–96

63 Grohmann, K., Hechtfischer, D.: 'Kryostromkomparatoren als Präzisionsstandards für rationale Gleich- und Wechselstromverhältnisse', *PTB-Mitteilungen*, 1982, **92**, (5/82), pp. 328–344

64 Seppa, H., Satrapinksi, A., Kiviranta, M., Virkki, V.: 'Thin-film cryogenic current comparator', *IEEE Trans. Instrum. Meas.*, 1999, **48**, (2), pp. 365–369

65 Elmquist, R.E., Dziuba, R.F.: 'High-temperature superconductor cryogenic current comparator', *IEEE Trans. Instrum. Meas.*, 1995, **44**, (2), pp. 262–264

66 Early, M.D., Jones, K., Staines, M.P., Exley, R.R.: 'Development of a split-toroid high-temperature superconducting cryogenic current comparator', *IEEE Trans. Instrum. Meas.*, 2001, **50**, (2), pp. 306–309

67 Giunchi, G., Bassani, E., Cavallin, T., Bancone, N., Pavese, F.: 'An MgB_2 superconducting shield for a cryogenic current comparator working up to 34 K', *Superconduct. Sci. Technol.*, 2007, **20**, pp. L39–L41

68 Elmquist, R.E.: 'Cryogenic current comparator measurements at 77 K using Thallium-2223 thick-film shields', *IEEE Trans. Instrum. Meas.*, 1999, **48**, (2), pp. 383–386

69 Hao, L., Macfarlane, J.C., Gallop, J.C.: 'Ion beam measurement with a high-temperature superconductor squid and current comparator', *IEEE Trans. Instrum. Meas.*, 2001, **50**, (2), pp. 302–305

70 Hao, L., Gallop, J.C., Macfarlane, J.C., Carr, C., Donaldson, G.B.: 'HTS flux concentrator for non-invasive sensing of charged particle beams', *Superconduct. Sci. Technol.*, 2001, **14**, pp. 1115–1118

71 Hao, L., Gallop, J.C., Macfarlane, J.C., Carr, C.: 'HTS cryogenic current comparator for non-invasive sensing of charged particle beams', *IEEE Trans. Instrum. Meas.*, 2003, **52**, (2), pp. 617–620

72 Watanabe, T., Watanabe, W., Ikeda, T., *et al.*: 'A prototype of a highly sensitive cryogenic current comparator with a HTS SQUID and HTS magnetic shield', *Supercond. Sci. Technol.*, 2004, **17**, pp. S450–S455

73 Milton, M.J.T., Williams, J.M., Forbes, A.B.: 'The quantum metrology triangle and the redefinition of the SI ampere and kilogram; analysis of a reduced set of observational equations', *Metrologia*, 2001, **47**, pp. 279–286

doi: 10.1049/iet-smt.2010.0170